

1 **The influence of particle geometry and the intermediate stress ratio**
2
3 **on the shear **behavior** of granular materials**
4
5
6
7

8 Y.H. Xie¹, Z.X. Yang^{2,*}, D. Barreto³, M.D. Jiang⁴
9

10 1. Postgraduate student, Department of Civil Engineering, Zhejiang University,
11 Hangzhou, Zhejiang, China, 310058, E-mail: xieyh@zju.edu.cn
12

13 2. Professor, Research Center of Coastal and Urban Geotechnical Engineering,
14 Department of Civil Engineering, Zhejiang University, Hangzhou, Zhejiang, China,
15 310058, E-mail: zxyang@zju.edu.cn; *corresponding author
16

17 3. Lecturer, School of Engineering and the Built Environment, Edinburgh Napier
18 University, Merchiston Campus, Edinburgh, EH10 5DT, Scotland, UK, E-mail:
19 D.Barreto@napier.ac.uk
20

21 4. Postgraduate student, Department of Civil Engineering, Zhejiang University,
22 Hangzhou, Zhejiang, China, 310058, E-mail: jiangmingdong@zju.edu.cn
23
24
25
26
27
28
29
30
31
32
33
34
35
36
37
38
39
40
41
42
43
44
45
46
47
48
49
50
51
52
53
54
55
56
57
58
59
60
61
62
63
64
65

The influence of particle geometry and the intermediate stress ratio on the shear **behavior** of granular materials

Y.H. Xie • Z.X. Yang • D. Barreto • M.D. Jiang

Abstract. The **behavior** of granular materials is very complex in nature and depends on particle shape, stress path, fabric, density, particle size distribution, amongst others. This paper presents a study of the effect of particle geometry (aspect ratio) on the mechanical behaviour of granular materials using the Discrete Element Method (DEM). This study discusses 3D DEM simulations of conventional triaxial and true triaxial tests. The numerical experiments employ samples with different particle aspect ratios and a unique particle size distribution (PSD). Test results show that both particle aspect ratio (AR) and intermediate stress ratio ($b=(\sigma_2'-\sigma_3')/(\sigma_1'-\sigma_3')$) affect the macro- and micro-scale responses. At the macro-scale, the shear strength decreases with an increase in both aspect ratio and intermediate stress ratio b values. At the micro-scale level, the fabric evolution is also affected by both AR and b . The results from DEM analyses qualitatively agree with available experimental data. The critical state behaviour and failure states are also discussed. It is observed that the position of the critical state loci in the compression ($e-p'$) space is only slightly affected by aspect ratio (AR) while the critical stress ratio is dependent on both AR and b . It is also demonstrated that the influence of the aspect ratio and the intermediate stress can be captured by micro-scale fabric evolutions that can be well understood within the framework of existing critical state theories. It is also found that for a given stress path, a unique critical state fabric norm is dependent on the particle shape but is independent of critical state void ratio.

Keywords: granular material, particle geometry, discrete element method, intermediate stress ratio, critical state, fabric evolution

1 Introduction

Granular materials are commonly encountered in nature and industry. For example, they are found in landslides and avalanches, as raw minerals for extraction and transport, cereal storage, powder mixing, etc. Cohesive frictional materials like concrete are also made of granulates [1]. The mechanical response of the granular materials is very complex and can be affected by confining pressure, density, stress path, particle shape, particle size distribution, amongst other factors [2-4]. It is widely **recognized** that particle characteristics affect the mechanical **behavior** of granular soils, which has been investigated extensively by experimental work. For example, Cho et al. [5] explored the effects of particle shape on packing density and on the small-to-large strain mechanical properties of sandy soils and found that the increasing particle irregularity causes an increase in the critical state angle of

Y.H. Xie • **M.D. Jiang**

Department of Civil Engineering, Zhejiang University, Hangzhou, Zhejiang, China

Z.X. Yang(✉)

Research Center of Coastal and Urban Geotechnical Engineering, Department of Civil Engineering, Zhejiang University,

Hangzhou, 310058 Zhejiang, China

e-mail: zxyang@zju.edu.cn

D. Barreto

School of Engineering and the Built Environment, Edinburgh Napier University, Merchiston Campus, Edinburgh, EH10 5DT, Scotland, UK

1 shearing resistance. Cavarretta et al. [3] and Yang and Luo [6] employed spherical glass beads and
2 crushed angular beads within mixtures including sand to explore the relationship between the critical
3 state **behavior** and particle shape. The latter experiments show that critical state **behavior** and
4 liquefaction potential are affected significantly by particle shape. Granular materials experience
5 different stress paths in nature [7]. Previous physical experiments and DEM simulations show that the
6 intermediate stress ratio ($b=(\sigma_2'-\sigma_3')/(\sigma_1'-\sigma_3')$) affects the soil response [8-10]. More recently, Xiao et al.
7 [11] performed a series of true triaxial experiments on coarse granular soil and found that b greatly
8 affects the critical state line in both $e-p'$ and $p'-q$ space. These findings are questionable as most
9 existing investigations unanimously confirm that the uniqueness of the critical state line (CSL) is
10 independent of stress paths. **In addition, careful scrutiny of the critical state data in the $e-p'$ plane by**
11 **Xiao et al. [11] indicates that the data points are indeed very sparse and the discrepancy between**
12 **different b cases for CSLs is insignificant, with the maximum void ratio difference only being less than**
13 **0.02 for $p'=200$ kPa. More critical state data are therefore required with a larger range of stresses and**
14 **void ratios in order to draw convincing conclusions.**

15
16
17
18
19 The Discrete Element Method (DEM) developed by Cundall and Strack [12] has **been** demonstrated
20 to be a promising tool to improve our understanding of the fundamental **behavior** of granular materials.
21 **A key feature of DEM simulations is that the same numerical sample can be subjected to different**
22 **stress paths, therefore the sample repeatability can be ensured in the simulation, whilst also**
23 **providing additional information which is not easily measured from physical experimental tests.**
24 In DEM simulations soil particles are idealized entities with spherical shape being the most common
25 type of particle geometry considered in 3D DEM simulations. Many DEM based numerical simulations
26 have been performed to investigate the effect of particle shape and intermediate stress ratio on the
27 mechanical **behavior** of granular media. Nouguiet et al. [13] performed 2D numerical simulations with
28 samples made of irregular hexagons with different particle elongation (i.e. ratio of maximum to
29 minimum length) and found that the angle of shearing resistance decreases as the particle elongation
30 increases for samples with the same initial density. Zhao et al. [14] used a composite (clumped) particle
31 model to create non-spherical particles and demonstrated that particle shape increased resistance to
32 compaction. Kumari and Sitharam [15] studied the effect of particle aspect ratio on the monotonic
33 shear **behavior**, but their study was limited to granular assemblies with only two aspect ratios but it
34 must be highlighted that the particle grading of these DEM specimens was not unique. More
35 importantly, their study only focused on the anisotropic responses in shear strength and the
36 corresponding microscopic **behavior**, while no analyses of the quantification of critical-state fabrics
37 were performed. Barreto and O'Sullivan [10] considered the effects of friction μ and the intermediate
38 stress ratio b under constant mean effective stress (p') and constant b fixed conditions to postulate the
39 mechanism that explains the effect of b on material response. Zhao and Guo [16] found that a unique
40 CSL in the $e-\log p'$ space, which **was then** confirmed by Yang and Wu [17] using anisotropic
41 assemblies consisting of clumped particles. Huang et al. [18] used DEM to understand the effect of b
42 on the critical state and discussed that the critical state line may not be unique, but the discrepancy
43 between different b cases for CSLs is not very significant and it might be argued that their results are
44 not accurate [17]. Bear in mind that the unique CSL assertion is derived from sound theoretical proof
45 [19]. Also note that the studies by Zhao and Guo [16] and Huang et al. [18] only considered spherical
46 particles. There is no prior research that systematically considers both particle shape and **generalized**
47 stress conditions such as those measured on true triaxial tests using DEM.

48
49
50
51
52
53
54
55
56
57
58
59 This study presents a comprehensive DEM analysis of particle aspect ratio effects on the
60
61
62
63
64
65

1 mechanical behavior of granular materials under generalized stress conditions. Shear strength,
2 dilatancy characteristics, critical state response, failure criterion, amongst other features of granular
3 materials' response are considered in this study. A series of DEM simulations including conventional
4 triaxial compression tests, as well as constant p' and constant b true triaxial tests are conducted in this
5 study, in which numerical specimens with varying aspect ratio but a unique particle size distribution are
6 considered. The main objective of this research was to investigate the critical state behavior of granular
7 assemblies composed by grains with varying AR s, when subjected to generalized stress conditions (i.e
8 not restricted to the triaxial space). Conventional triaxial compression tests under constant volume
9 (undrained) and constant cell pressure (drained) were performed to assess the effect of AR on peak
10 resistance and critical state behavior. Similarly, DEM simulations of true (drained) triaxial tests under
11 constant p' and different (constant) values of b were performed to assess the effect of both AR and b .
12 The effect of AR might (or not) refer to different granular materials, while the effect of b refers to the
13 effect of loading under generalized stress conditions. To differentiate these two effects, simulations sets
14 in which AR is kept constant were performed under different constant b values.
15
16
17
18
19
20

21 **2 Simulation details**

22 **2.1 Particle Characteristics**

23
24
25
26
27 Particle shape in granular materials is generally complex and often characterized by elongation,
28 roundness, angularity, texture, etc. [5]. In this study, the elongation of particle characterized by the
29 aspect ratio is considered. As illustrated in Fig. 1, the aspect ratio (AR) is defined as the ratio a_2/a_1
30 between the minor and major elongation axes. For a spherical particle, $AR=1$, and the higher the
31 particle elongation the smaller AR . For the numerical DEM samples used in this study, a power law size
32 distribution is chosen to generate particles to replicate a real sand grading and also avoid numerical
33 difficulties [20, 21]. As shown in Fig. 2, the particle size ranges vary between 0.4-1.2 mm equivalent
34 diameters. To assess the effect of the aspect ratio of the particles, clumped particles with varying
35 particle aspect ratio were created. To guarantee a fixed particle size distribution - PSD (Fig. 2) for all
36 numerical specimens the volume of individual particle clumps was set at the same value as for
37 spherical particles ($AR=1$). The uniformity coefficient D_{60}/D_{10} of the resulting PSD is 1.33. Three
38 different ratios were used for this study as illustrated in Table 1, which also shows their equivalent
39 radii.
40
41
42
43
44

45 **2.2 Simulation procedure**

46
47
48 The open source DEM code YADE [22] was used in this study. A standard linear contact model was
49 chosen. Its input parameters are listed in Table 2. A cubical assembly of particles with periodic
50 boundaries was adopted to assess granular material behavior free from boundary effects. Initially an
51 assembly of particles with no contacts between clumps was generated and then isotropically
52 compressed to a mean effective stress $p'=200$ kPa using a servo-control algorithm. A two-staged
53 compression was performed. In the first stage, to obtain varying densities of the samples, different
54 inter-particle friction coefficients were assigned onto the particles and the confining pressure was
55 gradually increased to 180 kPa. In the second stage, the inter-particle friction coefficient was restored
56 to a default value of $\mu=0.5$ and the confining pressure was then increased to 200 kPa. Static equilibrium
57
58
59
60
61
62
63
64
65

after compression was ensured by reaching an unbalanced force ratio lower than 0.001 as recommended by Kuhn et al. [23]. After this, conventional triaxial compression under both **constant cell pressure** and **constant volume** conditions were carried out. In addition, constant p' and constant b true triaxial simulations were also performed. In DEM simulations, density scaling is often used to reduce computational cost [1, 4, 24, 25]. Thornton and Antony [26] noted that the use of particle density scaling has no effect on the contact forces and displacements in case of quasi-static conditions. In this study, particle density was scaled up by a factor of 1,000. The selection of an appropriate strain rate is essential to ensure quasi-static conditions and maximize computational efficiency. Forterre and Pouliquen [27] state that in the quasi-static regime, the time required for macroscopic deformations is relatively large compared to that required for microscopic rearrangements, resulting in inertial number I ($= \dot{\gamma}d/\sqrt{P/\rho_p}$) values lower than 10^{-3} , where $\dot{\gamma}$ is the strain rate, d is the particle diameter, P is the relevant stress and ρ_p is the particle density. In addition to ensuring that $I \ll 10^{-3}$ for all simulations presented here, quasi-static conditions were verified by performing a preliminary parametric study using different strain rates. A strain rate of 0.05 s^{-1} was then selected for this study. To quantify the relative density (RD) of the samples, the maximum and minimal void ratios should be determined. According to Yang et al. [25], the maximum void ratio can be estimated by generating samples with inter-particle friction coefficient $\mu=0.5$, and the minimum void ratio is obtained with $\mu=0.0$, both under a reference state with confining pressure = 10 kPa.

3 Simulation results

In three dimensional analysis, the mean effective stress (p') and deviator stress (q) are defined as:

$$p' = (\sigma'_1 + \sigma'_2 + \sigma'_3) / 3 \quad (1)$$

$$q = \frac{1}{\sqrt{2}} [(\sigma'_1 - \sigma'_2)^2 + (\sigma'_2 - \sigma'_3)^2 + (\sigma'_1 - \sigma'_3)^2]^{0.5} \quad (2)$$

The term ‘fabric’ is frequently used to describe the microstructure of granular materials (e.g. [28]). From a microstructural perspective, for an aggregate having N measurements of the quantities that reflect the microstructure of the material, such as particle orientation, orientation of unit contact vectors, branch vectors, etc., the fabric can generally be represented by the deviatoric part \mathbf{F} of a tensor \mathbf{G} according to

$$\mathbf{F} = \frac{\mathbf{G}}{\text{tr}(\mathbf{G})/3} - \mathbf{1} \quad \text{with} \quad \mathbf{G} = \frac{1}{2N} \sum_{k=1}^{2N} w(\mathbf{m}^k) \mathbf{m}^k \otimes \mathbf{m}^k \quad (3)$$

where \mathbf{m}^k is a unit vector along the k^{th} measurement of the characteristic direction, say, the direction of contact unit normal [29], and $w(\mathbf{m}^k)$ is a weighting factor. If $w(\mathbf{m}^k)=1$ as in the case of a contact normal based definition of \mathbf{F} , $\text{tr}\mathbf{G}=1$. Here \mathbf{F} will be referred to as the fabric tensor. In order to identify the norm F and direction \mathbf{n}_F of \mathbf{F} , the following expressions can be invoked

$$\mathbf{F} = F\mathbf{n}_F \quad \text{with} \quad F = \sqrt{\mathbf{F}:\mathbf{F}}, \quad \mathbf{n}_F:\mathbf{n}_F = 1, \quad \text{tr}\mathbf{n}_F = 0 \quad (4)$$

The fabric tensor \mathbf{F} defined in this paper is a deviatoric tensor, and has two non-trivial invariants. We used the invariants norm F and the unit direction \mathbf{n}_F to represent the tensor \mathbf{F} , in which the norm F signifies the degree of fabric anisotropy. Therefore $F=0$ refers to isotropic fabric and $F > 0$ means the fabric is anisotropic.

A scaled version of \mathbf{F} defined in Eq. (3) is given in Eq. (5), which is widely used in the literature [16, 17, 21] to quantify the fabric anisotropy of soils. It is noted that the same symbol of \mathbf{F} is used in both Eq. (3) and Eq. (5) to avoid introducing more variables. The scaled \mathbf{F} has been referred to and used in the data interpretation for this paper.

$$\mathbf{F} = \frac{5}{2}(3\mathbf{G} - \mathbf{1}) \quad (5)$$

3.1 Triaxial compression results

Fig. 3 shows the macro-and micro behavior of DEM specimens sheared under constant volume (undrained) conditions. All the samples had the same initial density with relative density $D_r \approx 20\%$ and were isotropically compressed to 200 kPa, but with different particle aspect ratios. Fig. 3a illustrates the stress-strain response. At large strains ($\varepsilon_a \geq 40\%$) the deviatoric stress reached a constant value corresponding to a critical state that was dependent on the aspect ratio (AR). All the samples exhibit a hardening behavior and the maximum deviatoric stress decreases with an increase in AR . It can be seen from Fig. 3b that the effective stress path was also affected by particle shape. There was a contractive response prior to the dilative behavior with higher effective stress towards the critical state, as observed in real sands. This has been confirmed by the trends of the pseudo pore pressure for a dry packing, equivalent to the change in σ_3 , which is held constant in real undrained tests [21]. In terms of micro-scale response, Fig. 3c illustrates the evolution of the norm F of the fabric tensor \mathbf{F} . The norm F increases with axial strain, and reaches constant values at the critical state. Note that the fabric norm F decreases as AR increases. Fig. 3d illustrates the evolutions of the product of $\mathbf{n}:\mathbf{n}_F$ against the deviatoric strains, representing the relative orientation between fabric direction \mathbf{n}_F and stress direction \mathbf{n} . It is seen that unlike the fabric norm, $\mathbf{n}:\mathbf{n}_F$ increases with the strain and stabilizes at unity, indicating that the fabric direction is co-directional with the loading direction at the critical state. Similar results are also reported by Zhao and Guo [16], Yang and Wu [17].

Fig. 4 shows the results of triaxial compression under constant cell pressure (drained) conditions. In Fig. 4a the deviatoric stress reached a peak value followed by softening behavior. Once again, at large strains the deviatoric stresses became relatively constant and this can be considered as a critical state. This was confirmed by the constant volume conditions illustrated in Fig 4b at large strains. All the samples experience contraction followed by significant dilation. The evolution of fabric shown in Fig. 4c and 4d is consistent with that discussed for the constant volume conditions.

3.2 True triaxial (constant b) tests

Simulations with constant p' (=200 kPa) and constant b were also carried out using different values of AR . These sets of DEM simulations were carried out to differentiate the effects of both b and AR . Fig. 5 presents the true triaxial soil response of the sample with $AR=1$ and relative density $D_r \approx 20\%$ sheared under different constant b values. Fig. 5a shows that both the peak and critical deviatoric stresses decrease with increasing b value. This agrees with previous DEM and experimental studies [7, 11, 18]. The difference in initial shear stiffness appears to be insensitive to b value. Fig. 5b shows the volumetric responses, evidencing a dilative behavior for all values of b . The maximum dilation decreased as b increased as reported by Sazzad et al. [7] and Huang et al. [18]. Constant deviatoric stresses and volumetric strains at large strain $\varepsilon_a=30\%$, indicated that the critical state was reached. Fig. 5c shows that the fabric norm F increases with axial strain and it was nearly constant when $\varepsilon_a \geq 30\%$.

1 Although there were certain fluctuations, the norm F for $b=1$ was slightly higher than for $b=0$, as in
 2 previous studies [16, 17, 30]. Fig. 5d shows the evolutions of product of $\mathbf{n}:\mathbf{n}_F$. It became constant for
 3 all the b values, indicating that the fabric direction was co-directional with the loading direction at large
 4 strains.

5 Previous DEM research [10, 16, 18] has used spherical particles to study the influence of
 6 intermediate stress ratio on material response. We extend these studies by assessing the influence of
 7 particle shape due to different aspect ratios. DEM results for two additional sets of simulations
 8 including samples with $AR=0.833$ and $AR=0.714$ are also illustrated in Fig. 6 and Fig. 7, respectively.
 9 These are in addition to the simulation results with spherical particles ($AR=1.0$) shown in Fig. 5 for
 10 comparison purposes. Similar trends are observed for each of the AR values. It should be noted
 11 however that there is clear increase in maximum deviatoric and volumetric strains, which are solely
 12 due to the effect of AR . (i.e. there were smaller volumetric strains developed for simulations with $b =$
 13 1.0 and $AR = 1.0$ than for tests with $b = 1.0$ and $AR = 0.714$)

14 In geotechnical engineering, it is common to use $\varphi = \sin^{-1}[(\sigma_1' - \sigma_3') / (\sigma_1' + \sigma_3')]$ to define the shear
 15 strength of soils. The effect of AR and b on the angle of shearing resistance φ at the critical state is
 16 illustrated in Fig. 8 and φ decreases with AR for all the b values considered. There is also a maximum
 17 value around $b = 0.5$. The trends obtained here agree well with test data reported by Sutherland &
 18 Mesdary [31], Barreto and O'Sullivan [10], Thornton [32], amongst others. In this case, differentiation
 19 of the effects of b and AR is challenging, but there seems to be a larger effect of AR than b on φ for the
 20 three sets of simulations.

21 Previous studies [10, 30, 33] show that the DEM results compare well with the Lade and Duncan
 22 [34] failure criterion defined by:

$$23 \eta = \frac{I_1^3}{I_3} - 27 \quad (6)$$

24 in which $I_1 = \sigma_1' + \sigma_2' + \sigma_3'$ is the first stress invariant and $I_3 = \sigma_1'\sigma_2'\sigma_3'$ is the third stress invariant.

25 Fig. 9 presents the DEM results in the deviatoric plane together with their corresponding Lade and
 26 Duncan failure criterion. The agreement with the data is excellent. Barreto and O'Sullivan [10] reported
 27 that the Lade parameter η is a function of the inter-particle friction. As shown in Fig. 10, the Lade
 28 parameter η is also a function of AR with $\eta = 27.09 - 22.74AR$ in this study. Although very sparse data
 29 points indicate a simple linear function between AR and η , a convincing relationship could be obtained
 30 if more data points were available.

31 The fabric tensor can be manipulated in the same way as the stress tensor. Thornton [32] proposed
 32 a parameter η_f^* that determines the position of the fabric envelope in the deviatoric plane and is given
 33 by:

$$34 \eta_f^* = \frac{1}{2I_2^F - 3I_3^F} \quad (7)$$

35 where I_2^F and I_3^F are the second and third tensor invariants of the fabric tensor \mathbf{G} defined in Eq. (3).

36 Fig. 11 shows that the parameter defined by Eq. (7) agrees well with the data sets for differing
 37 aspect ratio. As shown in Fig. 12, there is also a linear relationship between η_f^* and AR , with

38 $\eta_f^* = 1.863 + 0.0554AR$, which, again, might be subjected to further verification by additional data.

The observation above is qualitatively consistent with the earlier DEM simulations on spherical particle assemblages by Zhao and Guo [16], Thornton and Zhang [30], and Thornton [32]. Recently, Li and Dafalias [35] have proved from theoretical perspective that the contour of the critical state fabric norm F_c on the π -plane is approximately reciprocal to the shape of critical state yield surface. In the present study, the norm ratio of the critical fabric tensor $F_c^{\text{TC}} / F_c^{\text{TE}}$ ranging from 1.06 to 1.10 for various AR values considered in this study, which is qualitatively found to be reciprocal to the ratio of critical stress ratios between TC and TE, i.e. $M_c^{\text{TC}} / M_c^{\text{TE}} = 1.23$. This observation is in agreement with previous numerical results by Thornton and Zhang [30] and Zhao and Guo [16] and the recent theoretical predictions by Li and Dafalias [35].

4 Critical state

The classical critical state theory (CST) developed by Roscoe et al. [36] and Schofield and Wroth [37] laid the foundations for critical state mechanics. The critical state is defined as the state of shear deformation without change in shear stress and volume and can be analytically expressed by:

$$\dot{p}' = 0, \quad \dot{\mathbf{s}} = 0, \quad \dot{\varepsilon}_v = 0 \quad \text{but} \quad \dot{\mathbf{e}} \neq 0 \quad (8)$$

in which p' is the mean normal effective stress, \mathbf{s} the deviatoric stress tensor, ε_v the volumetric strain, \mathbf{e} the deviatoric strain tensor, and a superposed dot denotes the rate. Upon reaching the critical state, the stress ratio $\eta = q/p$ and the void ratio e will satisfy the following conditions,

$$\eta = \eta_c = (q/p)_c = M \quad \text{and} \quad e = e_c = \hat{e}(p) \quad (9)$$

Li and Wang [38] proposed a linearization approach to straighten the critical state line (CSL) in the e - $(p'/p_a)^\xi$ plane for sand, which can be expressed as,

$$e_c = e_r - \lambda_c (p'/p_a)^\xi \quad (10)$$

where p_a is the atmospheric pressure serving as a reference pressure for normalization, e_r is the intersection of CSL on e -axis at $p'=0$, λ_c is the slope of the line and ξ is a parameter used for fine tuning for optimization. The parameter ξ is assumed to be 0.7 for simplicity.

In this study, additional conventional triaxial compression tests for each aspect ratio were conducted, with varying conditions such as density, confining pressure, and drainage conditions. From these results a critical state was identified and the relationship between AR and the critical state explored further.

Fig. 13 shows the critical state lines obtained from the above tests in the e - p' plane. It can be seen that simulation data can be fitted by the lines with the expressions given in Eq. (10) very well for each case. This demonstrates that the critical state for a given AR is independent of density, confining pressure and drainage conditions. The critical state lines converge, indicating that the influence of the particle aspect ratio is negligible when particle elongation continues to decrease. Yan and Dong [39] also discussed that the location of the critical state line in e - p' space is sensitive to particle grading. By incorporating the crushable particles in DEM simulation, Muir Wood and Maeda [40] found that the changing of particle grading can cause a downward parallel shift in the critical state line in e - p' space without change in slope. **Recently, the effect of particle breakage has been considered in critical state**

framework due to changes in the particle grading, which may occur in practical geotechnical engineering, e.g. pile driving and large earth-fill dams. Through experimental tests on sands, both Bandini and Coop [41] and Ghafghazi et al. [42] confirmed that the particle breakage can cause a shift of critical state line in e - p' space, while disagreed with the mode of position changes, i.e. translational offset or rotational shift. In the present study, the critical state line obtained in DEM results is lower in position than in the physical experiments. According to previous studies shown above, it can be interpreted due to the difference in grading of particles, the simplified particle shape modelled and/or due to particle crushing in the experimental tests which is ignored in these DEM simulations.

Fig. 14 presents the critical state line in the p' - q plane. The data points can be fitted by straight lines passing through the origin, with the slope of the straight line being the critical stress ratio M_c . For the sample with $AR=1$, which is composed of spherical particles, M_c has the smallest value = 0.770, which is consistent with the findings by Yan [43] and Gu et al. [44]. The critical state ratios for various AR are summarized in Fig. 15, and can be approximately fitted by a straight line, suggesting that samples with smaller AR (e.g. bigger elongation) have greater resistance to shear and result in large critical angles of shearing resistance. To verify this observation, the experiment data from Yang and Luo [6] are also added on this diagram, showing a similar qualitative trend between critical state ratio M_c and the particle aspect ratio AR , which ranges from 0.70 to 0.85 in their experiments.

Recently, an anisotropic critical state theory (ACST) was presented by Li and Dafalias [19] to enhance the classical CST by introducing a condition that fabric must satisfy at the critical state. According to Li and Dafalias [19], the norm F of \mathbf{F} evolves towards a unique critical state value while the direction \mathbf{n}_F evolves towards the loading direction. In addition, it has been shown that the fabric tensor \mathbf{F} should be a per-volume measure and the critical state norm of fabric tensor \mathbf{F} would be a function of Lode angle θ_F only, according to ACST [35]. However, \mathbf{F} defined by Eq. (5) using the measurements from DEM analysis might not be a per-volume measure and the easiest approach is to normalize \mathbf{F} with the specific volume v of the sample, which can be written as

$$\mathbf{F}' = \mathbf{F} / v = \mathbf{F} / (1 + e) \quad (11)$$

This lead to such normalized critical state fabric norm F'_c is a unique value and only depends on the tensor's Lode angle θ_F . It is noted that as specified in [17], the plastic part of the specific volume $v^p=(1+e^p)$ should be used to replace the total specific volume v in Eq. (11) as a rigorous normalizer. However, the elastic part of the void ratio is relatively insignificant and can be neglected for simplicity. Such treatment of using total specific volume will hardly affect the results presented in this paper.

Fig. 16(a) presents the critical values of F_c for the triaxial compression simulations considering varying AR values. It is seen that F_c depends on the particle shape, and the samples that composed of more elongated particles appear to have greater critical state norm, while the sample with spherical particles has lowest F_c . As expected, the un-normalized critical values of F_c paired with critical state e_c increase with the void ratio or density of the samples, as indicated by the dashed lines, confirming that the DEM fabric tensor defined in Eq. (5) is not a per-volume measure. However, the adaption of DEM fabric tensor by normalization given in Eq. (11) gives promising results, as illustrated in Fig. 16(b). For each AR , the critical values of F'_c can be interpreted independent of critical state e_c , with a horizontal straight dash line. This generate an average F'_c of 0.234 for $AR=1$, much lower than F'_c of 0.454 for $AR=0.833$ and F'_c of 0.502 for $AR=0.714$. Coefficient of variance (CoV) is used to quantify the degree of scatter of the normalized critical data deviating from the interpreted dashed trends. It is seen that CoV for $AR=1$ is 0.099, much greater than those for other two cases.

Bringing together the DEM simulation results up to the critical state with spherical particles available in literature [16, 44] are presented in Fig. 17(a) for the un-normalized critical state norm against e_c , indicating a polynomial trend with the F_c increasing with e_c , which is similar and consistent with the observations shown in Fig. 16(a). By applying the same normalization rule expressed in Eq. (13) for all the data from different DEM simulations indicate more scattered and biased data for $AR=1$ than those for other two cases. This is thought to be the coupling effects between specific volume v and the tensor's Lode angle on the critical state norm F_c [35], and the simple normalization rule expressed by Eq. (11) does not adequately tackle the adaption of DEM fabric tensor for samples involving spherical particles. Nevertheless, the particle shape dependent critical state fabric norm F'_c after normalization can reasonably satisfy the conditions advocated by anisotropic critical state theory.

5 Concluding Remarks

This paper presented a systematic DEM analysis of the effect of particle aspect ratio effects on the mechanical behavior of granular materials. A series of constant cell pressure and constant volume conventional triaxial compression tests, as well as constant p' and constant b true triaxial test numerical experiments were performed. DEM simulations considered specimens with varying aspect ratio, and a unique particle size distribution. It was shown that the aspect ratio of the particles has a significant influence on the shear strength, dilatancy and failure of granular materials. The microscopic responses were also examined in terms of the fabric evolutions during shear. Combined with the standard critical state theory (CST) and the recent anisotropic critical state theory (ACST), the critical state behavior was discussed. The main observations can be summarized as follows:

1. In DEM, clumped particles can be used to assess the effects of aspect ratio on granular material response. It was shown that while considering different initial densities and confining pressures, a critical state and fabric evolution can be attained.
2. Both conventional triaxial compression tests and constant p' and constant b true triaxial tests provided evidence that particle aspect ratio can significantly affect the stress-strain behavior of granular materials.
3. The η and η_f^* parameters that define the shape of failure criterion in principal stress and fabric space are a function of AR . The mobilized strength is a function of both AR and b .
4. It has been established that the particle aspect ratio can influence the critical state properties. The position of critical state line in e - p' plane is insensitive to particle aspect ratio. However, the critical state line in p' - q plane appears to be sensitive to particle aspect ratio.
5. In ACST, the critical fabric norm should be unique, that is only dependent on Lode angle θ_f of the stress path, for a given soil. The quantified fabric was adapted by a simple normalization that can reasonably satisfy this additional requirement by ACST. A unique critical state fabric norm was found whose magnitude is dependent on the particle shape but is independent of critical state void ratio.
6. Broad agreement of critical state fabric norm with those obtained from other DEM studies suggests that the simple normalization rule adopted in this study deserves further discussion when considering for samples composed of spherical particles.

Note that the particle shape in the present study is created by clumped particles with varying overlapping for simplicity. The effects of the convexity of particle shape and resulting resistance of

1 particle rotation are not considered and may have influence on the mechanical responses of the soils.
2 This could be improved by employing more realistic particle shapes in the DEM simulations. Such
3 work may involve complex algorithms and significant computational cost. Although this issue is out of
4 the scope of this paper, it deserves further investigation.
5

6 **Acknowledgement**

7
8
9 The research described was funded by the Natural Science Foundation of China (Grant Nos. 51578499,
10 51322809), the National Key Research and Development Program of China (No. 2016YFC0800204),
11 the National Key Basic Research Program of China (No. 2015CB057801), as well as funding by the
12 Royal Academy of Engineering under the Research Exchanges with China and India Scheme.
13
14

15
16 **Conflict of interest:** The authors declare that they have no conflict of interest.
17

18 **Reference**

- 19
- 20
- 21 1. O’Sullivan, C.: Particulate discrete element modelling: a geomechanics perspective. Applied
22 Geotechnics: Spon Press/Taylor & Francis, UK (2011).
- 23
- 24 2. Huang, Z.Y., Yang, Z.X., and Wang, Z.Y.: Discrete element modelling of sand behavior in a
25 biaxial shear test. Journal of Zhejiang University SCIENCE A, **9**(9), 1176-1183 (2008).
- 26
- 27 3. Cavarretta, I., Coop, M., and O’sullivan, C.: The influence of particle characteristics on the
28 behavior of coarse grained soils. Géotechnique, **60**(6), 413-423 (2010).
- 29
- 30 4. Yang, Z.X., Yang, J., and Wang, L.Z.: Micro-scale modeling of anisotropy effects on unbrained
31 behavior of granular soils. Granular Matter, **15**(5), 557-572 (2013).
- 32
- 33 5. Cho, G.C., Dodds, J., Dodds, J. and Santamarina, J.: Particle shape effects on packing density,
34 stiffness, and strength: natural and crushed sands. Journal of Geotechnical and Geoenvironmental
35 Engineering, **132**(5), 591-602 (2006).
- 36
- 37 6. Yang, J., and Luo, X.D.: Exploring the relationship between critical state and particle shape for
38 granular materials. Journal of the Mechanics and Physics of Solids, **84**, 196-213 (2015).
- 39
- 40 7. Sazzad, M. M., Suzuki, K., and Modaressi-Farahmand-Razavi, A. Macro-micro responses of
41 granular materials under different b values using DEM. International Journal of Geomechanics.
42 **12**(3), 220-228 (2012).
- 43
- 44 8. Yamada, Y., and Ishihara, K.: Anisotropic deformation characteristics of sand under three
45 dimensional stress conditions. Soils Found, **19**(2), 79 –94 (1979).
- 46
- 47 9. Wang, Q., and Lade, P. V.: Shear banding in true triaxial tests and its effect on failure in
48 sand. Journal of Engineering Mechanics, **127**(8), 754-761 (2001).
- 49
- 50 10. Barreto, D., and O’Sullivan, C: The influence of inter-particle friction and the intermediate stress
51 ratio on soil response under generalized stress conditions. Granular Matter, **14**(4), 505-521
52 (2012).
- 53
- 54 11. Xiao, Y., Sun, Y., Liu, H., and Yin, F.: Critical state behaviors of a coarse granular soil under
55 generalized stress conditions. Granular Matter, **18**(2), 1-13 (2016).
- 56
- 57 12. Cundall, P.A., and Strack, O.D.: A discrete numerical model for granular assemblies.
58 Géotechnique, **29**(1), 47-65 (1979).
- 59
- 60 13. Nouguier-Lehon, C., Cambou, B., and Vincens, E.: Influence of particle shape and angularity on
61 the behaviour of granular materials: a numerical analysis. International Journal for Numerical and
62
63
64
65

- Analytical Methods in Geomechanics, **27**(14), 1207-1226 (2003).
14. Zhao, T., Dai, F., Xu, N.W., Liu, Y., and Xu, Y.: A composite particle model for non-spherical particles in DEM simulations. *Granular Matter*, **17**(6), 763-774 (2015).
 15. Kumari, S.D.A., and Sitharam, T.G.: Effect of aspect ratio on the monotonic shear behavior: micromechanical interpretations. *Geotechnical and Geological Engineering*, **31**(5), 1543-1553 (2013).
 16. Zhao, J., and Guo, N.: Unique critical state characteristics in granular media considering fabric anisotropy. *Géotechnique*, **63**(8), 695-704 (2013).
 17. Yang, Z.X., and Wu, Y.: Critical state for anisotropic granular materials: a discrete element perspective. *Int. J. Geomech.*, 04016054 (2016).
 18. Huang, X., Hanley, K.J., O'Sullivan, C., Kwok, C.Y., and Wadee, M.A.: DEM analysis of the influence of the intermediate stress ratio on the critical-state behavior of granular materials. *Granular Matter*, **16**(5), 641-655 (2014).
 19. Li, X.S., and Dafalias, Y.F.: Anisotropic critical state theory: role of fabric. *J. Eng. Mech.*, **138**(3), 263-275 (2012).
 20. Mair, K., and Hazzard, J. F.: Nature of stress accommodation in sheared granular material: Insights from 3D numerical modelling. *Earth and Planetary Science Letters*, **259**(3), 469-485 (2007).
 21. Guo, N., and Zhao, J.: The signature of shear-induced anisotropy in granular media. *Comput. Geotech.* **47**, 1-15 (2013).
 22. Kozicki, J., and Donzé, F.V.: A new open-source software developed for numerical simulations using discrete modeling methods. *Computer Methods in Applied Mechanics and Engineering*, **197**(49-50), 4429-4443 (2008).
 23. Kuhn, M.R., Renken, H.E., Mixsell, A.D., and Kramer, S.L.: Investigation of cyclic liquefaction with discrete element simulations. *Journal of Geotechnical and Geoenvironmental Engineering*, **140**(12), 04014075 (2014).
 24. Thornton C, Antony S J.: Quasi-static deformation of particulate media. *Philosophical transactions-royal society of London series a mathematical physical and engineering sciences*, 2763-2782(1998).
 25. Yang, Z.X., Yang, J., and Wang, L.Z.: On the influence of inter-particle friction and dilatancy in granular materials: a numerical analysis. *Granular Matter*, **14**(13), 433-447 (2012).
 26. Thornton, C., and S. J. Antony.: Quasi-static shear deformation of a soft particle system. *Powder Technology*, 109(1-3),179-191(2000).
 27. Forterre, Y, and Pouliquen, O.: Granular flows. *Seminaire Poincare, XIII*, 69-100 (2009).
 28. Oda, M., and Iwashita, K.: *Mechanics of granular materials: an introduction*. CRC Pres, Netherlands (1999).
 29. Oda, M., Konishi, J., and Nemat-Nasser, S.: Experimental micromechanical evaluation of strength of granular materials: effects of particle rolling. *Mech. materials*, **1**(4), 269-283 (1982).
 30. Thornton, C., and Zhang, L.: On the evolution of stress and microstructure during general 3D deviatoric straining of granular media. *Géotechnique*, **60**(5), 333-341 (2010).
 31. Sutherland, H.B., and Mesdary, M.S.: The influence of the intermediate principal stress on the strength of sand. In *Proc of 7th Int Conf on Soil Mechanics and Foundation Engineering*, Vol. 1, 391-399 (1969).
 32. Thornton, C.: Numerical simulations of deviatoric shear deformation of granular

media. *Géotechnique*, **50**(1), 43-53 (2000).

33. Ng, T.T.: Shear strength of assemblies of ellipsoidal particles. *Géotechnique* **54**(10), 659-669 (2004).
34. Lade, P.V., and Duncan, J.M.: Elasto-plastic stress–strain theory for cohesionless soil. *Proc. ASCE*, **101**(10), 1037–1053 (1975).
35. Li, X.S., and Dafalias, Y.F.: Dissipation consistent fabric tensor definition from DEM to continuum for granular media. *J. Mech. Phys. Solids*, **78**, 141-153 (2015).
36. Roscoe, K.H., Schofield, A., and Worth, C.P.: On the yielding of soils. *Géotechnique*, **8**(1), 22-53 (1958).
37. Schofield, A., and Wroth, P.: *Critical state soil mechanics*. McGraw-Hill, New York (1968).
38. Li, X.S., and Wang, Y.: Linear representation of steady-state line for sand. *J. Geotech. Geoenviron. Eng.*, **124**(12), 1215-1217 (1998).
39. Yan, W. M., and Dong, J.: Effect of particle grading on the response of an idealized granular assemblage. *International Journal of Geomechanics*, **11**(4), 276-285 (2011).
40. Wood, D.M., and Maeda, K.: Changing grading of soil: effect on critical states. *Acta Geotechnica*, **3**(1), 3-14 (2008).
41. Bandini, V., and COOP, M.R.: The influence of particle breakage on the location of the critical state line of sands. *Soils and foundations*, **51**(4), 591-600 (2011).
42. Ghafghazi, M., Shuttle, D.A., & DeJong, J.T.: Particle breakage and the critical state of sand. *Soils and Foundations*, **54**(3), 451-461 (2014).
43. Yan, W.M.: Fabric evolution in a numerical direct shear test. *Computers and Geotechnics*, **36**(4), 597-603 (2009).
44. Gu, X., Huang, M., & Qian, J.: DEM investigation on the evolution of microstructure in granular soils under shearing. *Granular Matter*, **16**(1), 91-106 (2014).

Figure captions

- 1
2 **Fig. 1** Definition of particle aspect ratio AR
3 **Fig. 2** Particle size distribution of assemblages employed in this study
4 **Fig. 3** Effect of ARs on **constant volume compression** behavior of granular assembly ($p'_0=200$ kPa,
5 $D_r\sim 20\%$): (a) Deviatoric stress vs. axial strain; (b) Effective stress path; (c) Fabric norm vs. axial
6 strain; (d) $\mathbf{n}:\mathbf{n}_F$ vs. axial strain
7 **Fig. 4** Effect of ARs on **constant cell pressure compression** behavior of granular assembly ($p'_0=200$ kPa,
8 $D_r\sim 20\%$): (a) Deviatoric stress vs. axial strain; (b) Volume strain vs. axial strain; (c) Fabric norm
9 vs. axial strain; (d) $\mathbf{n}:\mathbf{n}_F$ vs. axial strain
10 **Fig. 5** Effect of b on behavior of granular assembly ($AR=1$, $p'_0=200$ kPa, $D_r\sim 20\%$): (a) Deviatoric stress
11 vs. axial strain; (b) Volume strain vs. axial strain ; (c) Fabric norm vs. axial strain; (d) $\mathbf{n}:\mathbf{n}_F$ vs.
12 axial strain
13 **Fig. 6** Effect of b on behavior of granular assembly ($AR=0.833$, $p'_0=200$ kPa, $D_r\sim 20\%$): (a) Deviatoric
14 stress vs. axial strain; (b) Volume strain vs. axial strain ; (c) Fabric norm vs. axial strain; (d) $\mathbf{n}:\mathbf{n}_F$
15 vs. axial strain
16 **Fig. 7** Effect of b on behavior of granular assembly ($AR=0.714$, $p'_0=200$ kPa, $D_r\sim 20\%$): (a) Deviatoric
17 stress vs. axial strain; (b) Volume strain vs. axial strain ; (c) Fabric norm vs. axial strain; (d) $\mathbf{n}:\mathbf{n}_F$
18 vs. axial strain
19 **Fig. 8** Effect of ARs on angle of shearing resistance
20 **Fig. 9** Effect of ARs on state surface of critical stress in deviatoric plane
21 **Fig. 10** Effect of ARs on the η parameter
22 **Fig. 11** Effect of ARs on state surface of critical fabric in deviatoric plane
23 **Fig. 12** Effect of ARs on the η^* parameter
24 **Fig. 13** Critical state line at $e-p'$ plane
25 **Fig. 14** Critical state line at $p'-q$ plane
26 **Fig. 15** Effect of ARs on the critical stress ratio
27 **Fig. 16** Critical-state fabric norm against void ratio for triaxial compression tests
28 (a) Un-normalized norm; (b) Normalized norm
29 **Fig. 17** Critical state fabric norm for compression tests with spherical particles ($AR=1$)
30 (a) Un-normalized norm; (b) Normalized norm
31
32
33
34
35
36
37
38
39
40
41
42
43
44
45
46
47
48
49
50
51
52
53
54
55
56
57
58
59
60
61
62
63
64
65

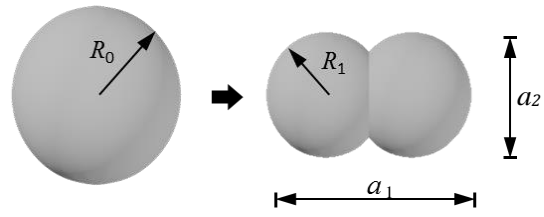


Fig. 1 Definition of particle aspect ratio AR

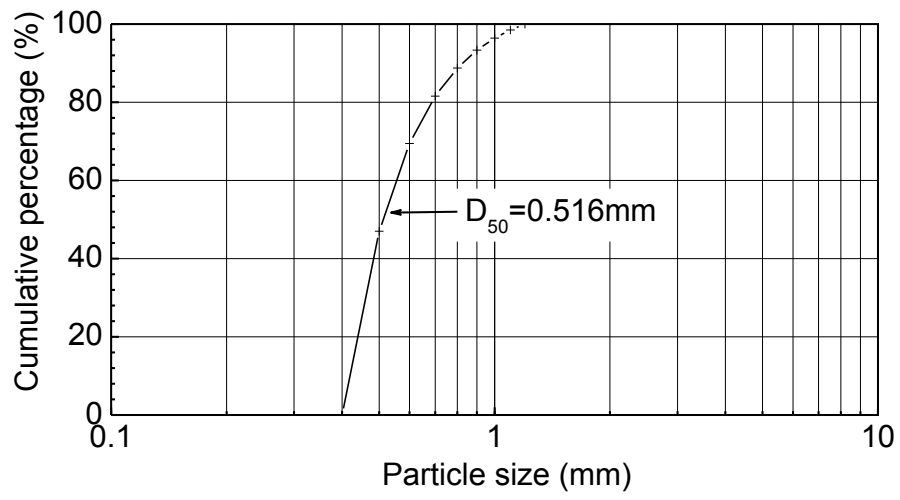


Fig. 2 Particle size distribution of assemblages employed in this study

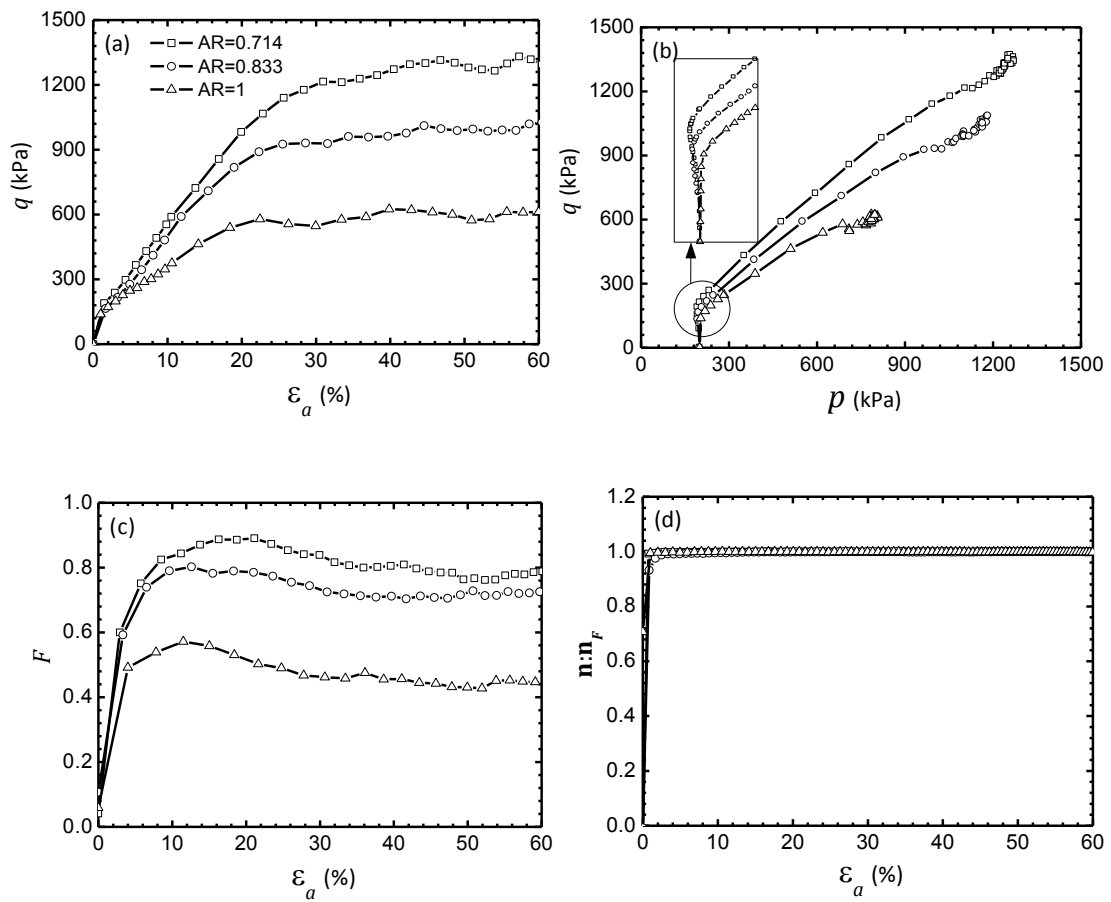


Fig. 3 Effect of ARs on constant volume compression behavior of granular assembly ($p'_0=200$ kPa, $D_r \sim 20\%$): (a) Deviatoric stress vs. axial strain; (b) Effective stress path; (c) Fabric norm vs. axial strain; (d) $\mathbf{n}:\mathbf{n}_F$ vs. axial strain

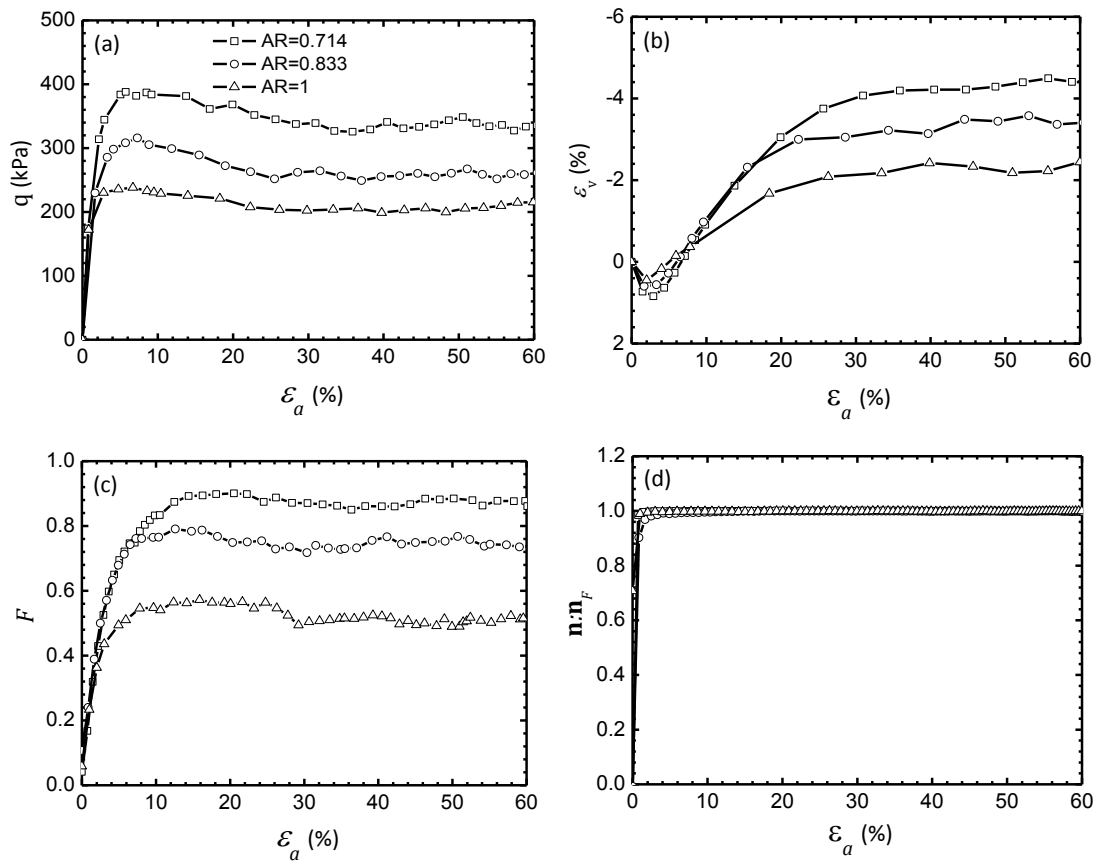


Fig. 4 Effect of ARs on **constant cell pressure compression** behavior of granular assembly ($p'_0=200$ kPa, $D_r \sim 20\%$): (a) Deviatoric stress vs. axial strain; (b) Volume strain vs. axial strain; (c) Fabric norm vs. axial strain; (d) **$n:n_F$** vs. axial strain

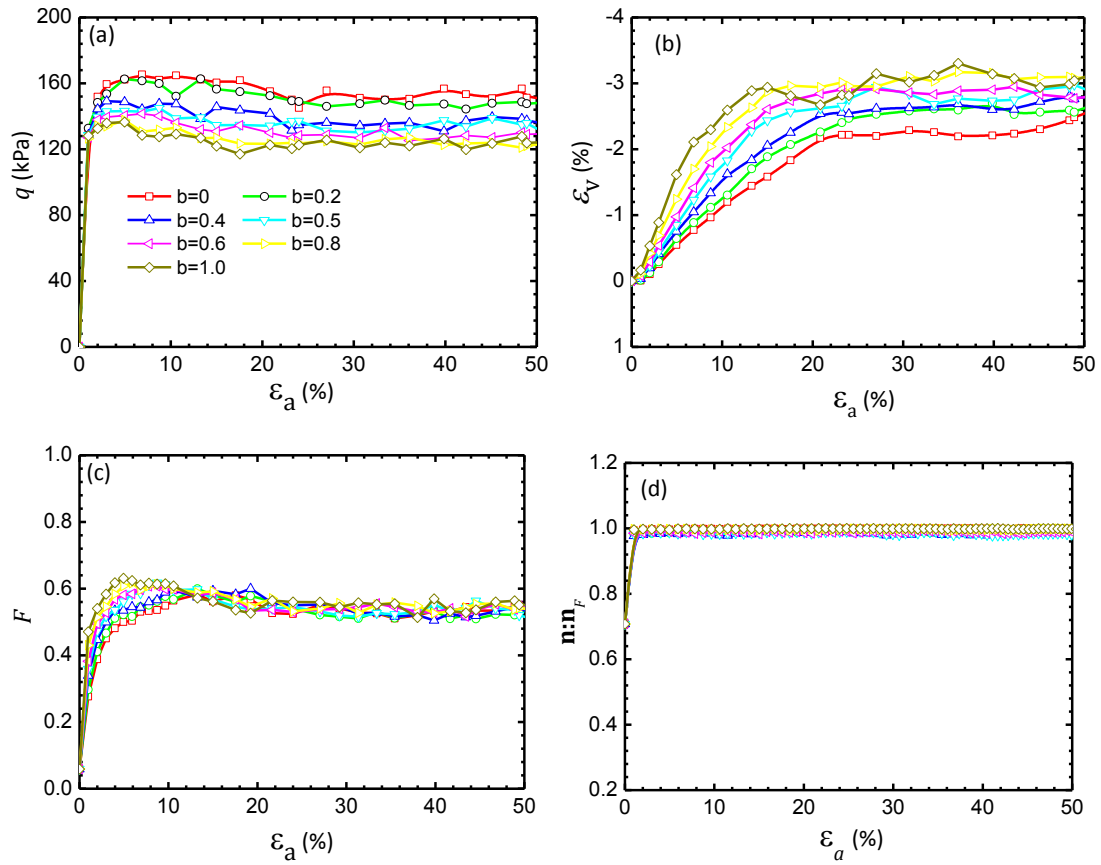


Fig. 5 Effect of b on behavior of granular assembly ($AR=1$, $p'_0=200$ kPa, $D_r\sim 20\%$): (a) Deviatoric stress vs. axial strain; (b) Volume strain vs. axial strain ; (c) Fabric norm vs. axial strain; (d) $\mathbf{n}:\mathbf{n}_F$ vs. axial strain

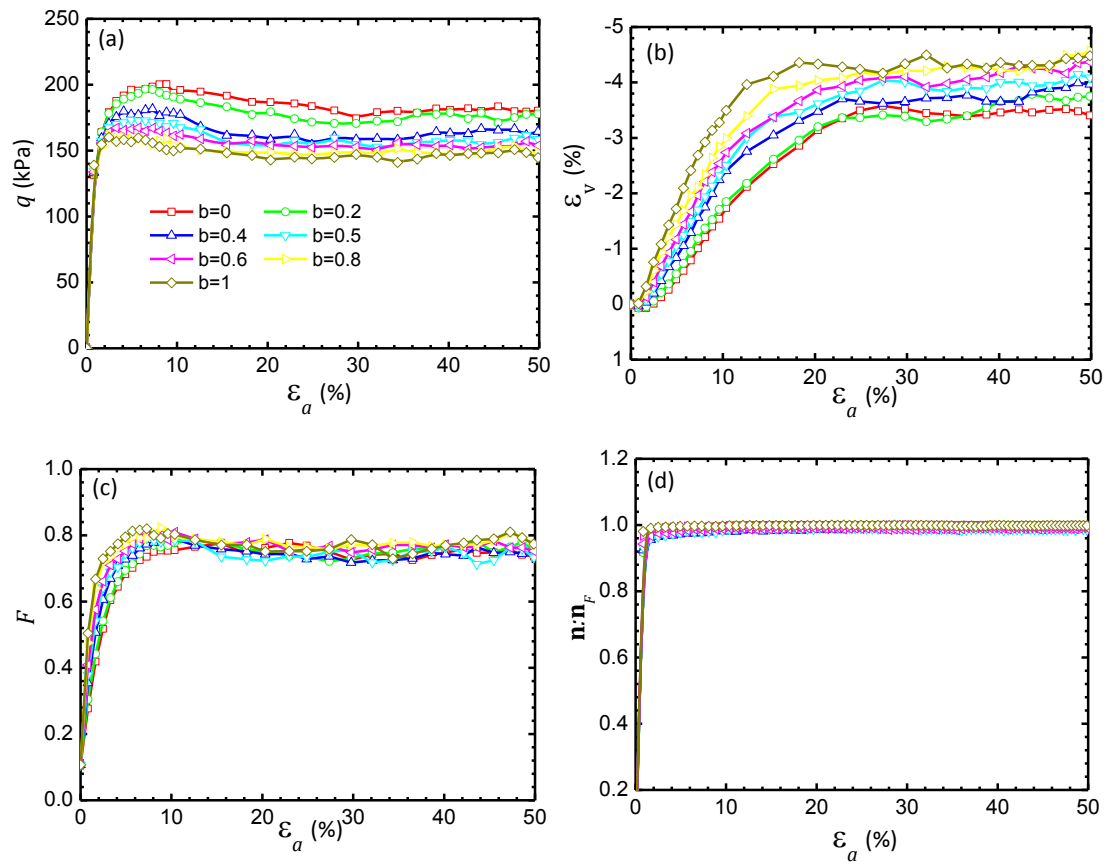


Fig. 6 Effect of b on behavior of granular assembly ($AR=0.833$, $p'_0=200$ kPa, $D_r \sim 20\%$): (a) Deviatoric stress vs. axial strain; (b) Volume strain vs. axial strain; (c) Fabric norm vs. axial strain; (d) $\mathbf{n}:\mathbf{n}_F$ vs. axial strain

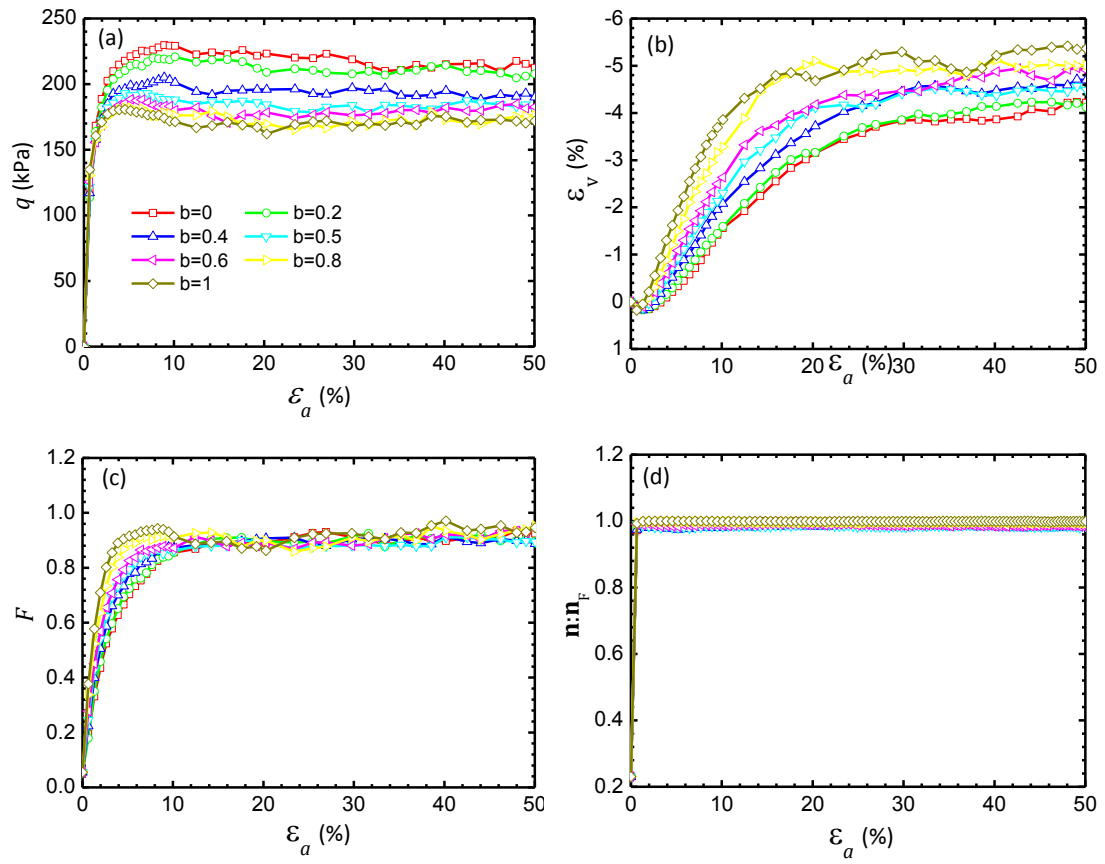


Fig. 7 Effect of b on behavior of granular assembly ($AR=0.714$, $p'_0=200$ kPa, $D_r \sim 20\%$): (a) Deviatoric stress vs. axial strain; (b) Volume strain vs. axial strain ; (c) Fabric norm vs. axial strain; (d) $\mathbf{n}:\mathbf{n}_F$ vs. axial strain

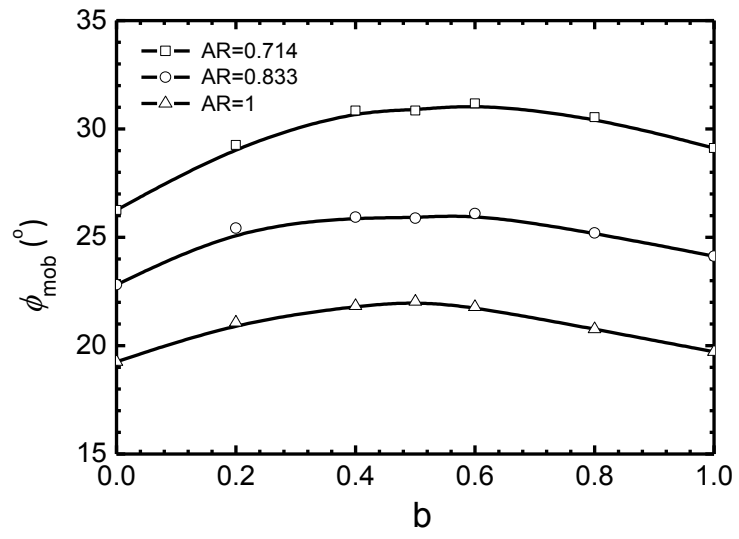


Fig. 8 Effect of ARs on angle of shearing resistance

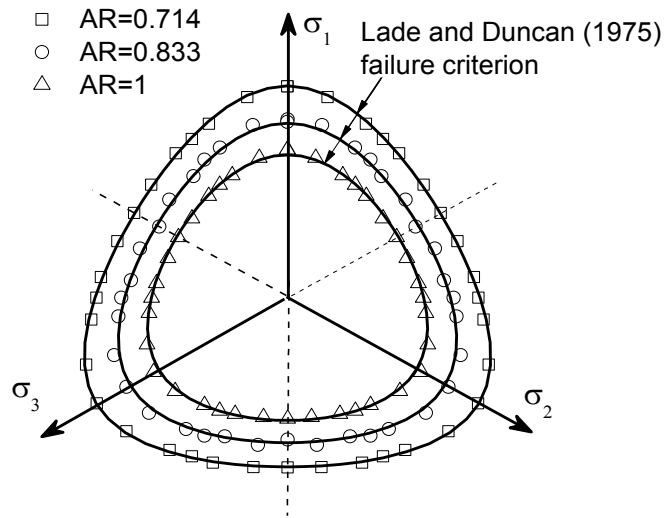


Fig. 9 Effect of ARs on state surface of critical stress in deviatoric plane

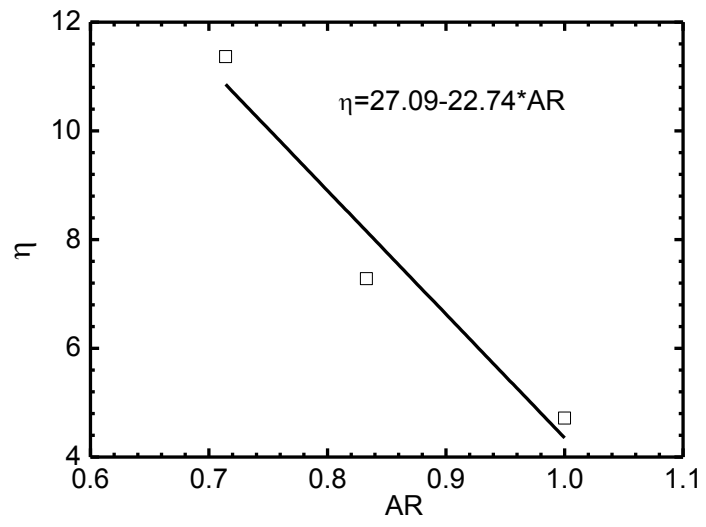


Fig. 10 Effect of ARs on the η parameter

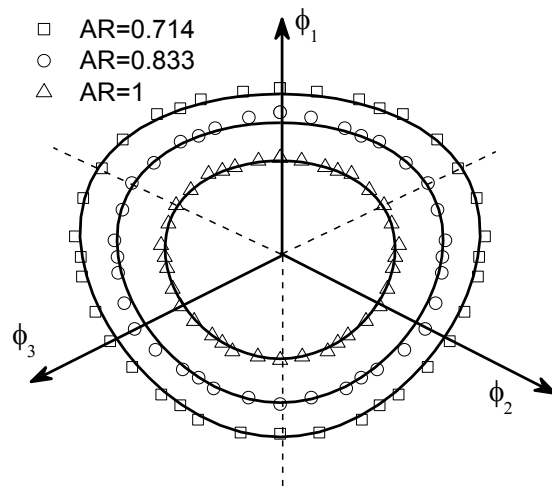


Fig. 11 Effect of ARs on state surface of critical fabric in deviatoric plane

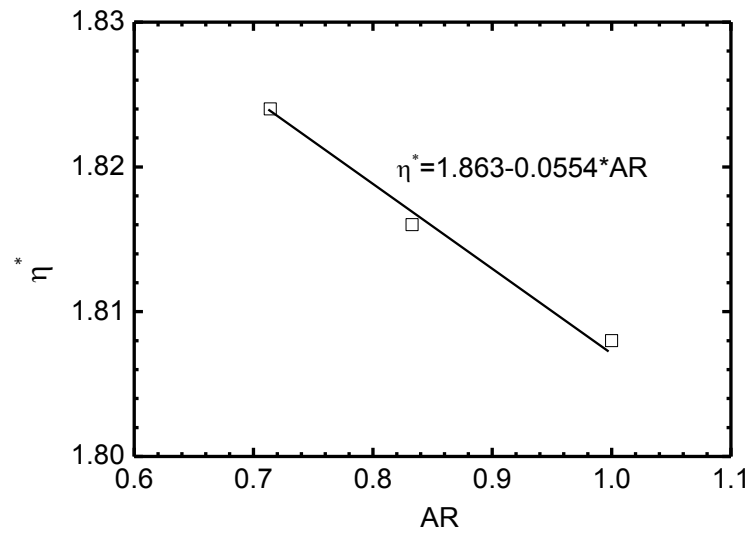
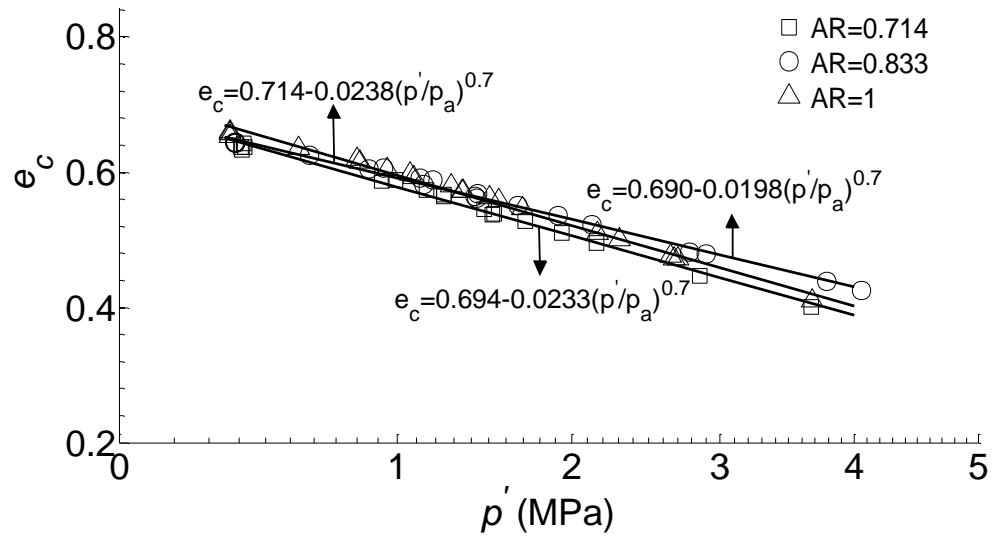


Fig. 12 Effect of ARs on the η^* parameter



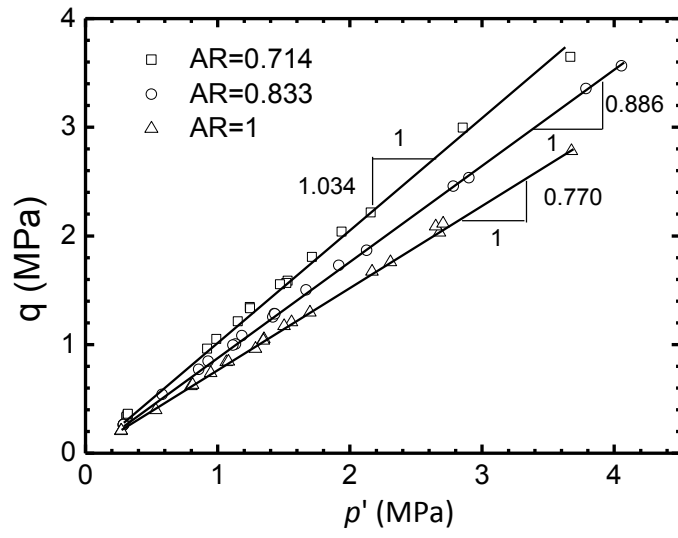


Fig. 14 Critical state line at p' - q plane

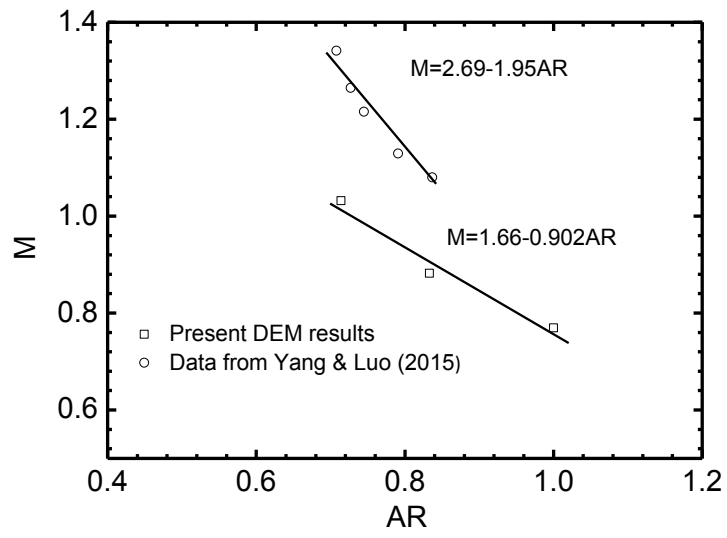


Fig. 15 Effect of ARs on the critical stress ratio

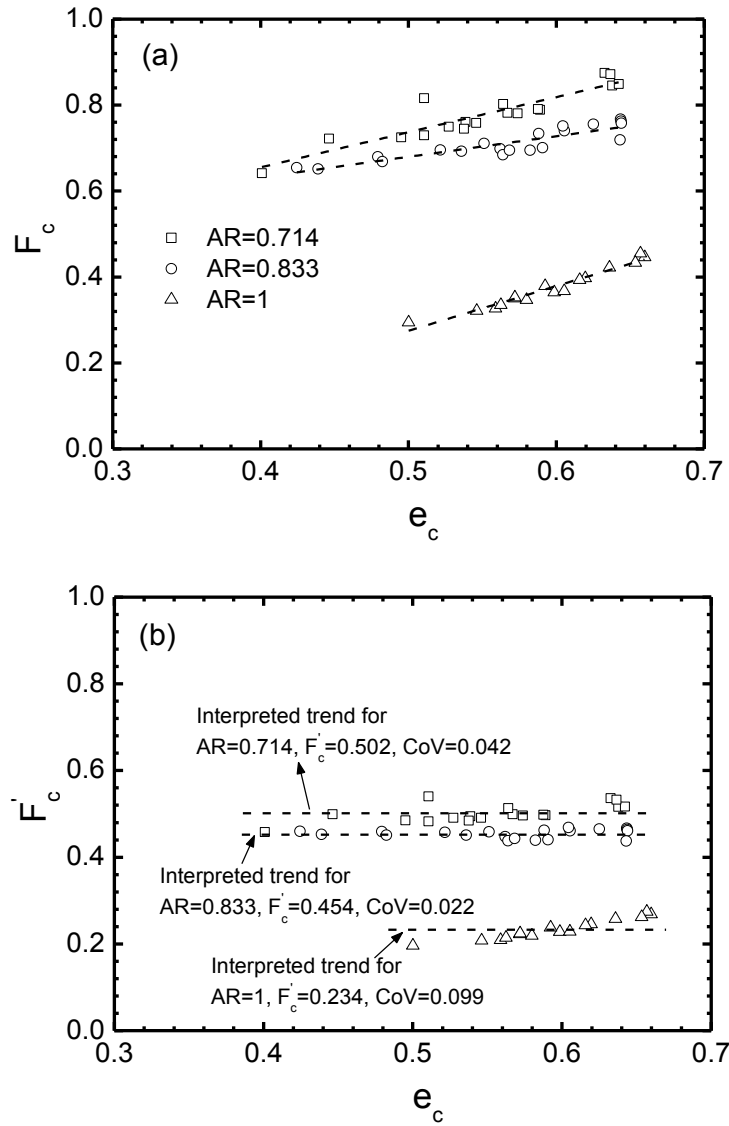


Fig. 16 Critical-state fabric norm against void ratio for triaxial compression tests
 (a) Un-normalized norm; (b) Normalized norm

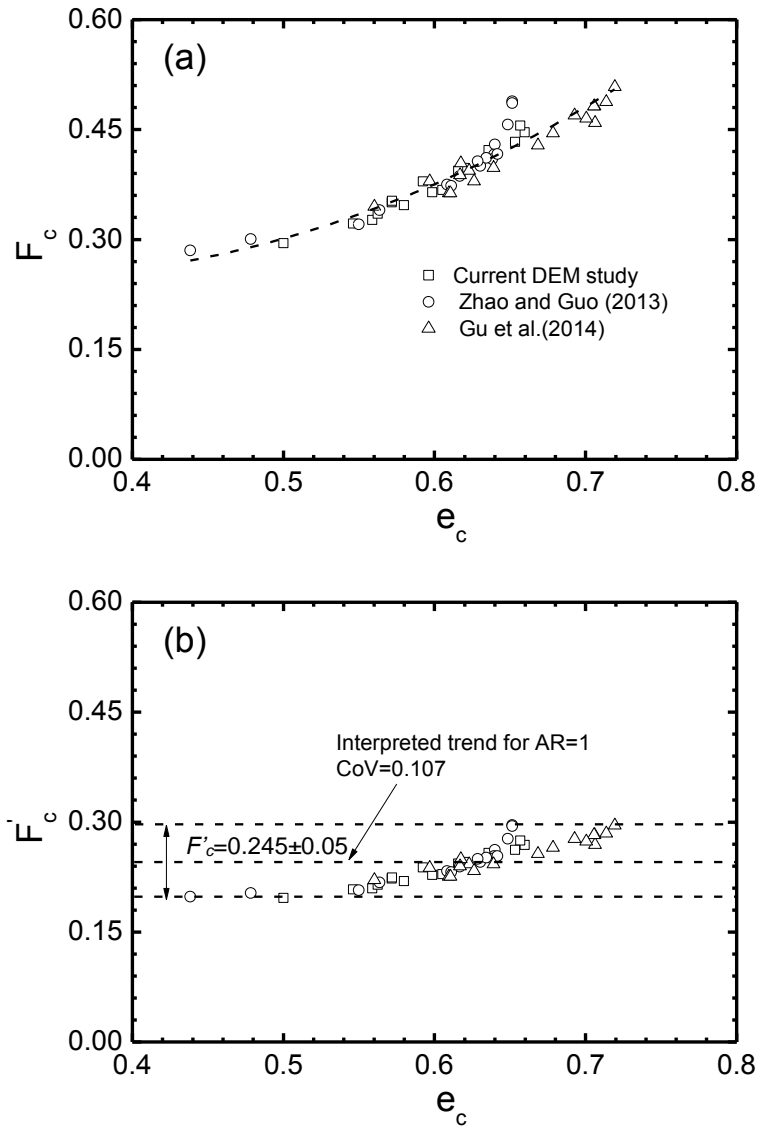


Fig. 17 Critical state fabric norm for compression tests with spherical particles (AR=1)
 (a) Un-normalized norm; (b) Normalized norm

Table 1 Particle aspect ratio AR




Shape	AR	Equivalent radius R
	1	r
	0.833	1.09r
	0.714	1.162r

Table 2 DEM Parameters used in the simulations

Sample ID	AR=0.714	AR=0.833	AR=1
Particle density (10^6 kg/m ³)	2.65	2.65	2.65
Normal stiffness K_n/d (MPa)	100	100	100
Tangential stiffness K_s/d (MPa)	100	100	100
Relative density D_r (%)	20.4	20.2	20.8
Damping ratio	0.001	0.001	0.001
Unbalanced force ratio	0.001	0.001	0.001
Number of clumps N	10000	10000	10000
Initial confining pressure p'_0 (kPa)	200	200	200
Strain rate (s ⁻¹)	0.05	0.05	0.05